A Single-Switch Flyback-Current-Fed DC–DC Converter

Peter Mantovanelli Barbosa, *Member, IEEE,* and Ivo Barbi, *Senior Member, IEEE*

***Abstract*—This work presents a novel dc–dc converter, whose significant advantages are the single power switch, single-input inductor, purely capacitive output filter, isolation, low current ripple through the output capacitor, and operation at constant frequency in a conventional pulse-width-modulation scheme. The new converter operates over a wide input-voltage range and can be employed in power factor correction and multiple-output power supplies. Theoretical analysis is presented along with experimental results taken from a laboratory prototype rated at 300 W/50 kHz.**

***Index Terms*— DC–DC converters, flyback converters, high frequency, power supplies.**

NOMENCLATURE

- γ Normalized output current.
- λ Normalized voltage across capacitor C_b.
- β Normalized voltage.
- a Flyback inductor turns ratio.
- D Duty cycle.
- f_s Switching frequency.
- i_m Instantaneous transformer magnetizing current.
- I_m Transformer average magnetizing current.
- I_o Average output current.
- I_s Flyback inductor average magnetizing current.
- i_s Instantaneous flyback inductor magnetizing current.
- k Inductance factor.
- L_m Magnetizing inductance of the transformer.
- L_s Magnetizing inductance of the flyback inductor.
- n Transformer turns ratio.
- T_s Switching period.
- V_c Average voltage across capacitor C_b.
- $V_{\rm in}$ Input-voltage source.
- V_o Output voltage.

I. INTRODUCTION

THE FLYBACK-current-fed push–pull topology [1]–[4], shown in Fig. 1, has several advantages when used in high-power and high-voltage applications. It has one single-input inductor, but no output inductor, which makes it a good choice for a multiple-output power supply with one or more high-voltage outputs. The series flyback inductor provides inherent current protection against transformer saturation.

Manuscript received October 16, 1996; revised September 9, 1997. Recommended by Associate Editor, T. Sloane.

P. M. Barbosa is with the Department of Electrical Engineering, Federal University of Paraná, 81531-970, Curitiba, PR, Brazil.

I. Barbi is with the Institute of Power Electronics, Federal University of Santa Catarina, 88040-970, Florianópolis, SC, Brazil.

Publisher Item Identifier S 0885-8993(98)03339-0.

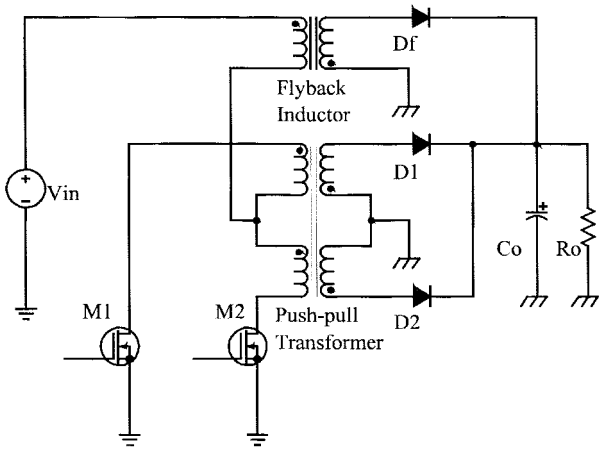

Fig. 1. Flyback-current-fed push–pull converter.

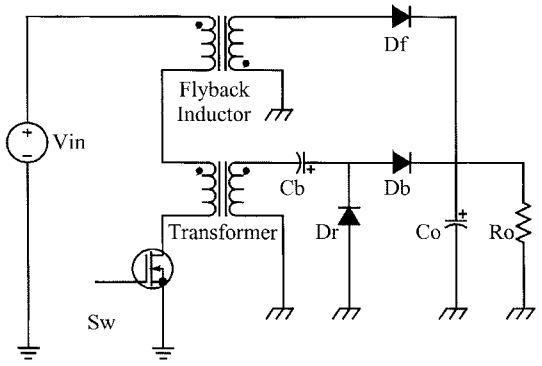

Fig. 2. Proposed single-switch flyback-current-fed topology.

The power converter in Fig. 1 combines the characteristics of the buck and boost converters in a single power stage of conversion. Therefore, it can be applied to operate over a wide input-voltage range and can be used in power factor correction. The ability of correcting the power factor and regulating the output voltage in a single power stage increases the overall efficiency of the power supply, reduces the total volume, size, and final cost of the product.

The aforementioned converter has another advantage when operating in buck mode: low current ripple through the output capacitor because either the rectifier diodes of the transformer or the rectifier diode of the flyback inductor are delivering energy to the output. Current ripple causes losses in the series equivalent resistance (SRE) of the electrolytic capacitors. Thus, a low current ripple avoids overheating of the device and prolongs its useful life.

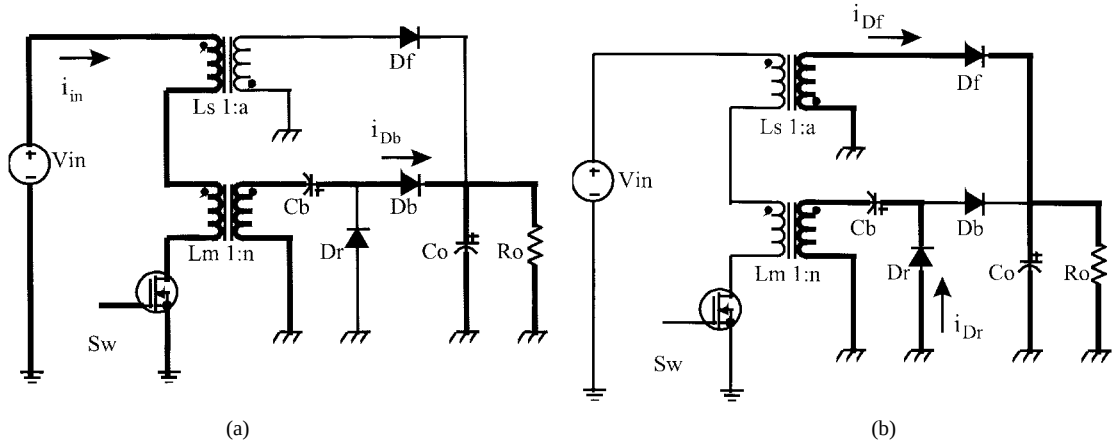

Fig. 3. Basic operation of the single-switch flyback-current-fed converter in the CCM.

One disadvantage of this converter, for low-power applications, is the need for two power switches to operate properly. In this paper, a single-switch flyback-current-fed converter is proposed. In spite of using only one switch, it retains the major advantages of the two switches converter.

II. The New Topology and Principle of Operation

The power diagram of the single-switch flyback-current-fed topology is shown in Fig. 2. The circuit has only one flyback inductor for any number of outputs, one transformer with volt-second balance ensured by capacitor C_b, and a single power switch S_w. The proposed converter is appropriate for operation from 0% up to 100% switch duty cycle. The converter also presents a low current ripple through capacitor C_o because in the continuous conduction mode (CCM) either diodes D_b or D_f are turned on.

The basic operation in the CCM can be described as follows. At the switch gated-on interval, the equivalent circuit assumed by the converter is shown in bold in Fig. 3(a). The magnetizing current of the flyback inductor flows from the input-voltage source. Both magnetizing currents increase linearly during this interval. In the CCM operation, the magnetizing current of the flyback inductor is always larger than the magnetizing current of the transformer. For this reason, diode D_b is turned on. Therefore, energy is being transferred from the input-voltage source to the output section, represented by capacitor C_o and load R_o. At the end of DT_s, switch S_w is gated off, so the converter assumes the equivalent circuit shown in bold in Fig. 3(b). The energy previously stored in the magnetizing inductance of the flyback inductor is delivered through diode D_f to the output section. During the same interval, the transformer is demagnetized through diode D_r and capacitor C_b and both magnetizing currents decrease linearly.

Fig. 4 shows typical converter waveforms in the CCM. During the switch gated-on interval, we can see in Fig. 4(f) that the magnetizing currents of the magnetic devices increase linearly. Fig. 4(b) and (f) shows in bold the input current and the current through diode D_b, respectively, reflected to the primary side of the transformer. As can be verified in Fig. 4(f), when S_w is gated on, diode D_b conducts the difference between the magnetizing currents i_s and i_m. During the switch gated-off interval, diode D_f conducts the magnetizing current of the flyback inductor and diode D_r conducts the magnetizing current of the transformer. Fig. 4(a) and (d) represents the voltage across the primary side of the flyback inductor and transformer, respectively.

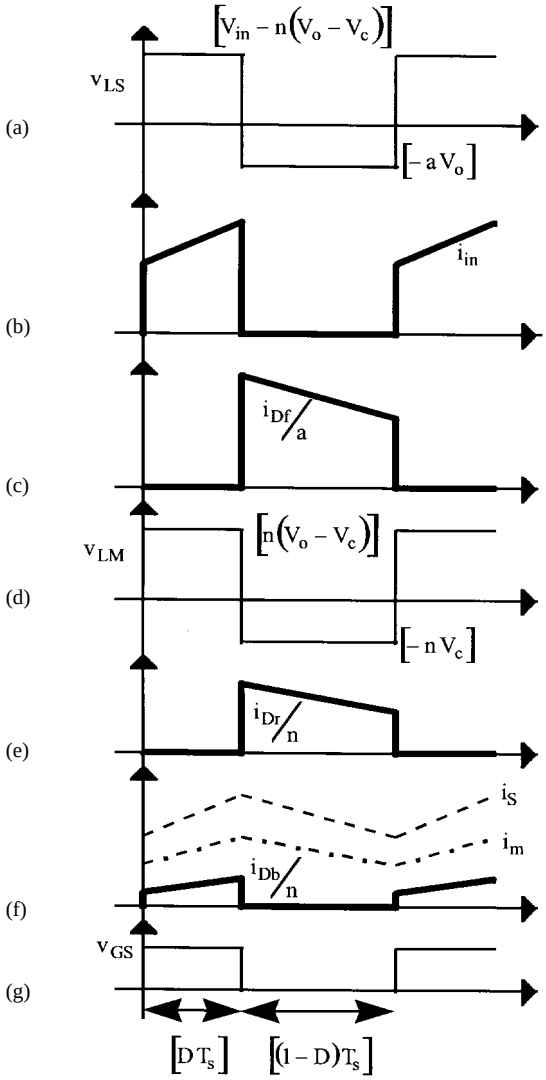

Fig. 4. Typical waveforms presented by the proposed converter in the CCM.

III. Power Sharing Between the Transformer and Flyback Inductor

The energy transferred from the input-voltage source to the output section is shared between the flyback inductor and the transformer. The following analysis determines a mean of dividing the output power equally between the magnetic devices.

The power transferred through the transformer to the load can be calculated as

$$P_{\text{trans}} = V_o I_b. \tag{1}$$

From the converter topology, we can see that the average current through diodes D_b and D_r is the same. The average current through diode D_r is given by $I_r = nI_m(1-D)$. In the proposed converter, I_m has the same value of the average input current I_{in}. Thus, substituting the relationships of this paragraph in (1) results

$$\begin{aligned} P_{\text{trans}} &= V_o I_b = V_o I_r \\ &= V_o n I_m (1-D) \\ &= n(1-D) V_o I_{\text{in}}. \end{aligned} \tag{2}$$

Similarly, we can write the power transferred from the input to the load through the flyback inductor as

$$P_{\text{fly}} = V_o I_f \tag{3}$$

where I_f is the average current through D_f given by $I_f = aI_s(1-D)$.

During the switch gated-on interval, S_w conducts the magnetizing current i_s of the flyback inductor. Thus, the average current through S_w is calculated by $I_{\text{sw}} = DI_s$. From the topology, we can observe that $I_{\text{sw}} = I_m = I_{\text{in}}$, resulting I_s as follows:

$$I_s = I_{\text{in}}/D. \tag{4}$$

From (3) and (4), we can obtain the power transferred through the flyback inductor to the load

$$\begin{aligned} P_{\text{fly}} &= V_o I_f = V_o a I_s (1-D) \\ &= a\left(\frac{1-D}{D}\right) V_o I_{\text{in}}. \end{aligned} \tag{5}$$

To obtain the relationship between P_{trans} and P_{fly}, we can divide (2) by (5)

$$\frac{P_{\text{trans}}}{P_{\text{fly}}} = \frac{n}{a} D. \tag{6}$$

For $a = n$ in (6), the power transferred through the transformer to the load is lower than the power transferred through the flyback inductor. If we want to equalize the power to be transferred from the input-voltage source to the load between the magnetic devices, it is necessary to ensure the following relationship:

$$\frac{a}{n} = D. \tag{7}$$

Expression (7) is a theoretical limit. However, in the CCM, to produce a given output voltage, there is a fixed duty-cycle value and consequently a fixed ratio between a and n.

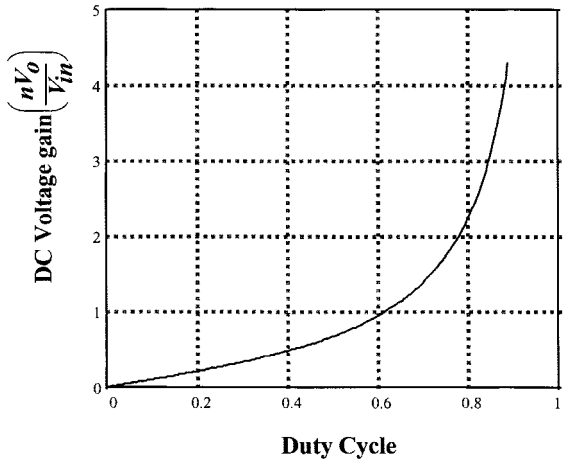

Fig. 5. Voltage conversion ratio (dc voltage gain) of the proposed converter.

IV. Voltage Conversion Ratio and Output Characteristics

Neglecting the parasitic elements, the voltage conversion ratio can be easily derived as follows. From Figs. 3 and 4, during the switch gated-on interval, the voltage applied across the primary side of the flyback inductor is given by $V_{LS} = [V_{\text{in}} - n(V_o - V_c)]$ and across the transformer by $V_{LM} = [n(V_o - V_c)]$. Similarly, when S_w is gated off, the voltage across the primary of the flyback inductor is $V_{LS} = [-aV_o]$, while the transformer is subjected to $V_{LM} = [-nV_c]$.

To operate properly, there must be flux balance in the magnetic devices. Thus

$$[V_{\text{in}} - n(V_o - V_c)]DT_s = aV_o(1-D)T_s \tag{8}$$

$$n(V_o - V_c)DT_s = nV_c(1-D)T_s. \tag{9}$$

From (8) and (9) result

$$V_c = V_{\text{in}} \frac{D^2}{(1-D)(nD+a)} \tag{10}$$

$$\frac{V_o}{V_{\text{in}}} = \frac{D}{(1-D)(nD+a)}. \tag{11}$$

Expression (10) gives us the average voltage across capacitor C_b, necessary to ensure magnetic flux balance in the transformer. Expression (11) represents the converter voltage conversion ratio (the dc voltage gain) and is graphically depicted in Fig. 5 for $a = n$.

From Fig. 5, we can notice that the proposed converter has a dc voltage gain that can be changed from zero $(D = 0)$ up to infinite $(D = 1)$. The proposed converter, as the flyback-current-fed push–pull topology, has the property of operating in both modes: buck and boost. Such property makes the single-switch converter suitable to be employed in power factor correction and in applications that require operation over a wide input-voltage range as well.

In the proposed converter, discontinuous conduction mode (DCM) is characterized when the magnetizing current of the magnetic devices achieves zero during the switch gated-off interval or when the magnetizing current of the transformer

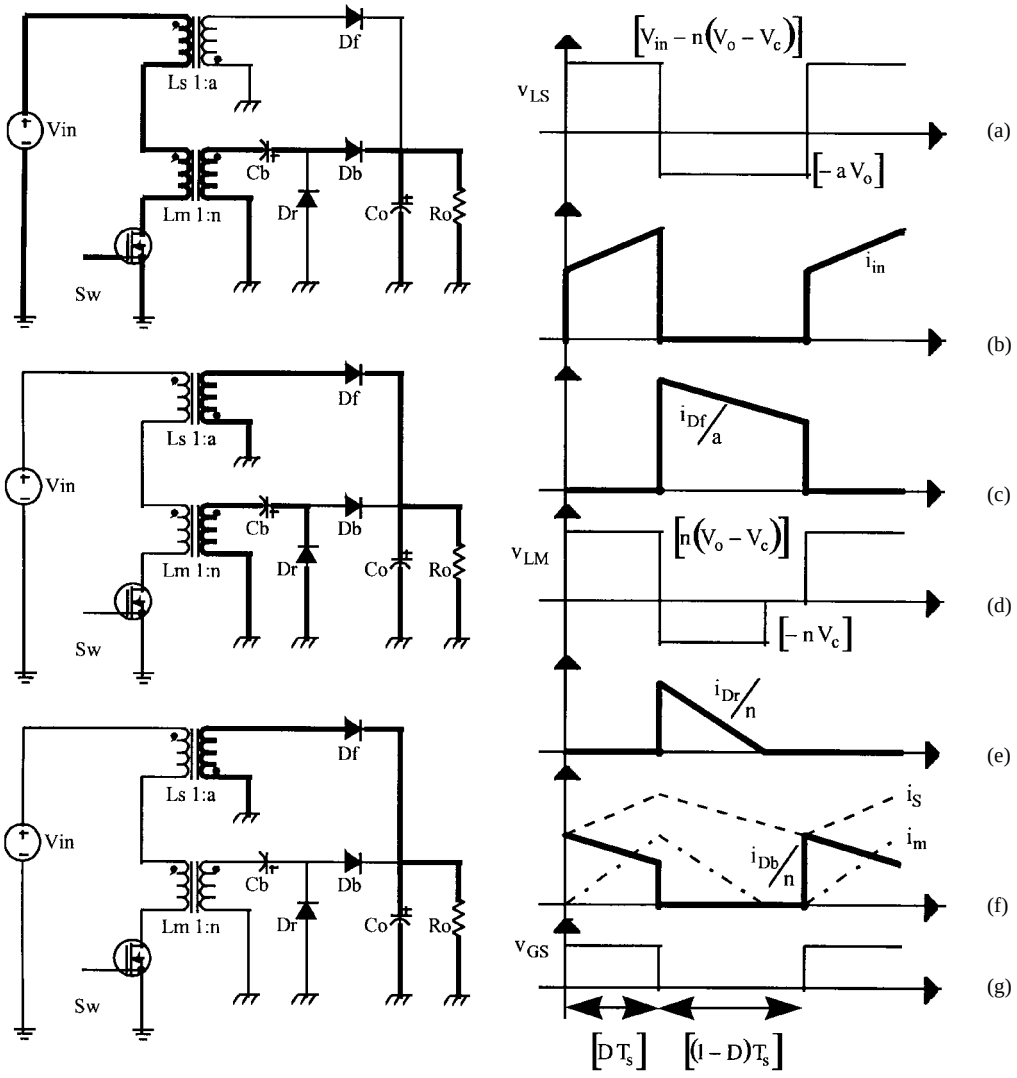

Fig. 6. Discontinuous conduction mode—case I.

achieves the magnetizing current of the flyback inductor during the switch gated-on interval. Thus, we can identify three different cases of discontinuity.

- Case I: The magnetizing current of the transformer achieves zero during the switch gated-off interval, blocking diode D_r. Fig. 6 shows the operation stages and the main converter waveforms.
- Case II: The magnetizing current of the transformer achieves the magnetizing current of the flyback inductor during the switch gated-on interval, blocking diode D_b, and achieves zero when S_w is gated off, forcing diode D_r to be blocked. Circuit operation and main waveforms are depicted in Fig. 7.
- Case III: Both magnetizing currents achieve zero during the switch gated-off interval, blocking diodes D_r and D_f. Fig. 8 shows the operation.

The final expressions that describe the operation of the converter in the DCM are shown below in Table I.

The normalized variables were defined as follows:

$$\begin{aligned} \beta &= V_o'/V_{\text{in}} \quad \gamma = I_o' L_s f_s / V_{\text{in}} \\ \lambda &= V_c'/V_{\text{in}} \quad k = L_m/L_s. \end{aligned} \tag{12}$$

To obtain the output characteristics, we must combine the complete behavior of the converter for all modes of operation (CCM and DCM). These curves are graphically depicted in Fig. 9. They represent the normalized output voltage (β) as a function of the normalized output current (γ), taking the duty cycle (D) as a parameter and for various values of the inductance factor (k). The normalized output voltage and current are reflected to the primary side of the transformer. In order to equalize the power transferred from the input-voltage source to the output load between the magnetic devices, the turns ratio of the flyback inductor has been taken as $a = nD$ for all curves.

Analyzing the theoretical output characteristics in Fig. 9, we verify that if the inductance factor k is increased, the operation range in the DCM decreases. Hence, if it is needed to operate the converter over a wide CCM range, the inductance factor must be chosen as high as possible.

TABLE I
EXPRESSIONS DESCRIBING THE BEHAVIOR OF THE CONVERTER IN THE DCM

Case of Discontinuity	Normalized Voltage Across Capacitor C_b (λ)	Normalized Output Voltage (β)
Case I	$\lambda = -D^3 \dfrac{n}{\left[(2akD - 2nkD - 2ak)\gamma - anD^2 + anD^3\right]}$	$\beta = \left(-nD^2 - 2k\gamma\right) \dfrac{D}{\left[(2akD - 2nkD - 2ak)\gamma - anD^2 + anD^3\right]}$
Case II	$\lambda = \dfrac{(aD\beta + D - a\beta)^2}{\left[a^2\beta(1-D)^2(2+k) + 2k\gamma - 2aD(1-D)\right]}$	$\beta = \dfrac{-D(2akD + 2nD + nkD - 2ak) - 2k^2\gamma}{Q(a,n,k,D,\gamma)}$ $Q(a,n,k,D,\gamma) = a^2k(2+k) - 2nk(1+k)\gamma + \ldots$ $+ a(2nk + ak^2 + 2ak + 2n)D^2 - \ldots$ $- 2a(ak^2 + nk + n + 2ak)D$
Case III	$\lambda = \dfrac{1}{2}n \dfrac{D^4}{\left(nD^2(1+k) + 2k\gamma\right)\gamma}$	$\beta = \dfrac{1}{2}\left(nD^2 + 2k\gamma\right) \dfrac{D^2}{\left(nD^2(1+k) + 2k\gamma\right)\gamma}$

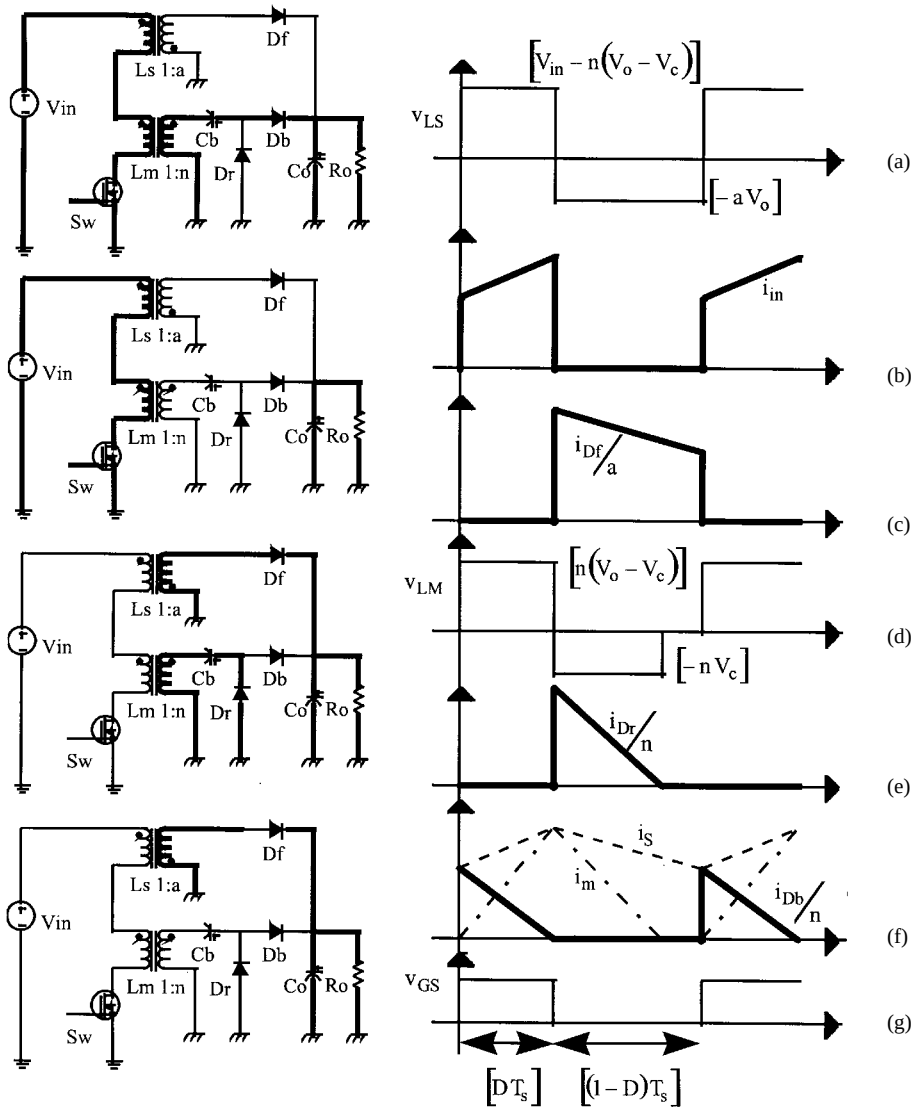

Fig. 7. Discontinuous conduction mode—case II.

V. DESIGN PROCEDURE AND EXAMPLE

To illustrate the design procedure, an example is presented in this section, whose main specifications are:

input-voltage source: $V_{\text{in}} = 300$ V;
output voltage: $V_o = 56$ V;
maximum output power: $P_o = 300$ W;
minimum output power: $P_{\text{min}} = 60$ W;
switching frequency: $f_s = 50$ kHz;
switch voltage: $V_{\text{sw}} = 500$ V.

A. Duty Cycle

The duty cycle is chosen taking into account the voltage applied across the power switch. In the CCM, during the switch gated-off interval, S_w is subjected to the voltage given

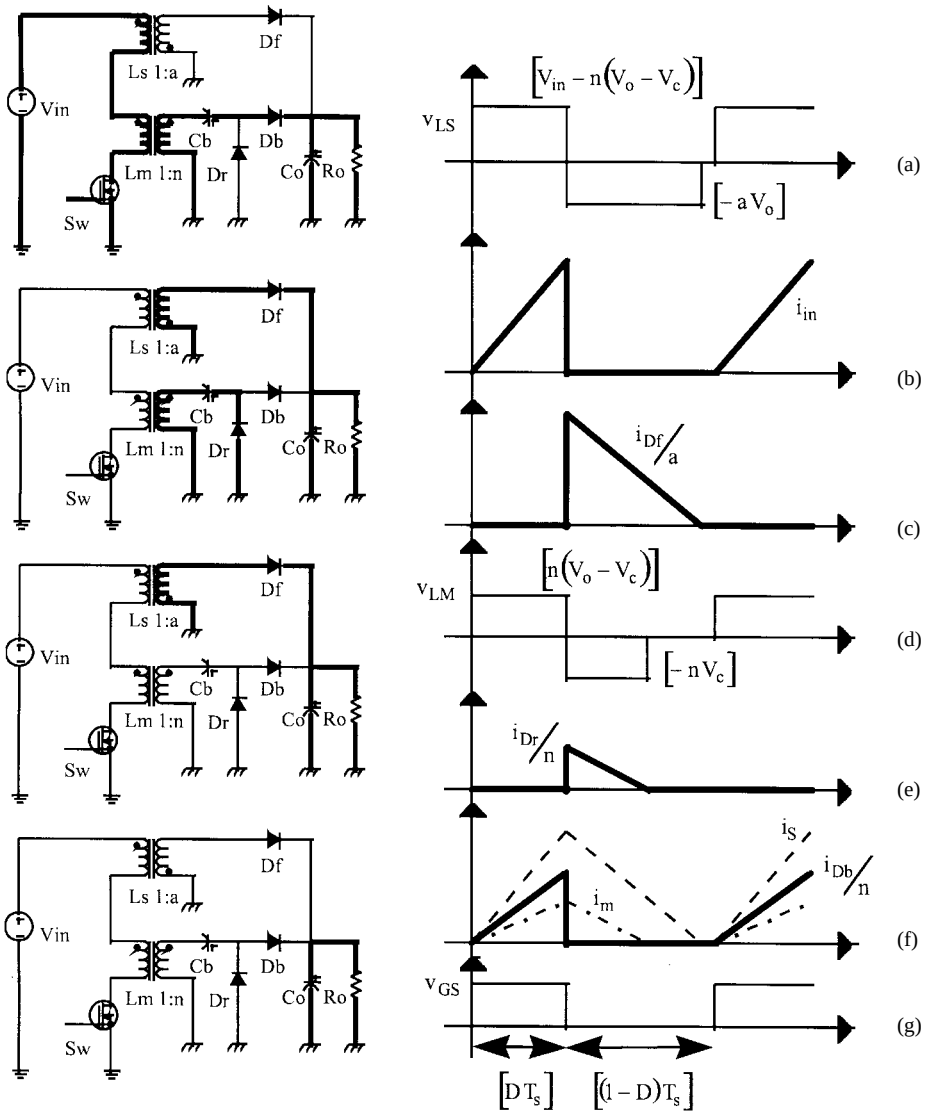

Fig. 8. Discontinuous conduction mode—case III.

by $V_{sw} = V_{in} + aV_o + nV_c$. Substituting (10) and (11) into the last expression yields

$$V_{sw} = \frac{V_{in}}{1-D}. \tag{13}$$

The voltage applied across S_w is independent of a and n. Solving for the duty cycle

$$D = \frac{V_{sw} - V_{in}}{V_{sw}} = \frac{500 - 300}{500} = 0.4.$$

B. Turns Ratio

To share equally the output power at full load between the magnetic devices, we must take $a = nD$. Substituting $a = nD$ in (11) and solving for n results

$$n = \frac{V_{in}}{2V_o(1-D)} = \frac{300}{2 \times 56 \times (1 - 0.4)} = 4.464$$
$$a = nD = 4.464 \times 0.4 = 1.786.$$

C. Magnetizing Inductances L_s and L_m

Taking the inductance factor $k = 0.5$, the calculated duty cycle $D = 0.4$, and forcing the converter to operate in the CCM at minimum power, results, from Fig. 9(c), $\gamma_{min} = 0.24$. The minimum output current reflected to the primary side of the transformer is calculated below

$$I'_{omin} = \frac{P_{min}}{nV_o} = \frac{60}{4.464 \times 56} = 240 \text{ mA}.$$

We can calculate L_s and L_m from the definition of the normalized output current as follows:

$$L_s = \frac{\gamma_{min} V_{in}}{I'_{omin} f_s} = \frac{0.24 \times 300}{0.24 \times 50 \times 10^3} = 6 \text{ mH}$$
$$L_m = kL_s = 0.5 \times 6 \times 10^{-3} = 3 \text{ mH}.$$

D. Decoupling Capacitor C_b

The average voltage across C_b is obtained from (10)

$$V_c = V_{in} \frac{D^2}{(1-D)(nD+a)}$$
$$V_c = 300 \times \frac{0.4^2}{(1-0.4) \times (4.464 \times 0.4 + 1.786)} = 22.4 \text{ V}.$$

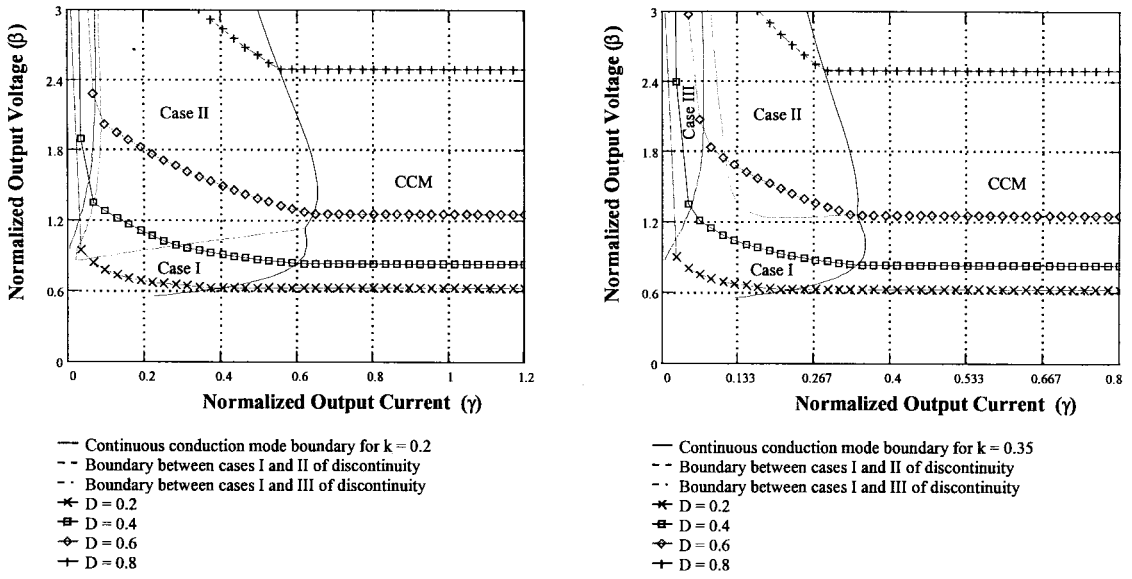

(a)

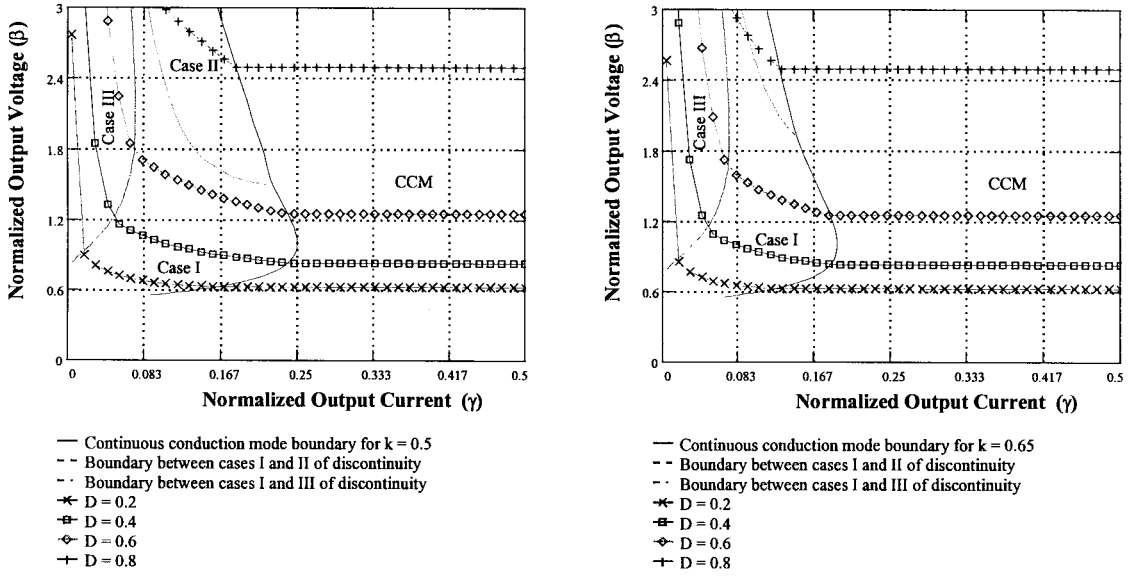

(b)

Fig. 9. Theoretical output characteristics of the single-switch flyback-current-fed topology.

Specifying the voltage ripple for C_b as 15% of V_c results

$$C_b = n(1-D)\frac{P_o}{\Delta V_c V_{\text{in}} f_s}$$

$$C_b = 4.464 \times (1-0.4) \times \frac{300}{0.15 \times 22.4 \times 300 \times 50 \times 10^3}$$

$$C_b \cong 15\ \mu\text{F}.$$

E. Output Capacitor C_o

Specifying the voltage ripple for the output voltage as 1% of its average value results:

$$C_o = P_o \frac{n(1-D)V_o - DV_{\text{in}}}{V_{\text{in}} V_o \Delta V_o f_s}$$

$$C_o = 300 \times \frac{4.464 \times (1-0.4) \times 56 - 0.4 \times 300}{300 \times 56 \times 0.01 \times 56 \times 50 \times 10^3}$$

$$= 22\ \mu\text{F}.$$

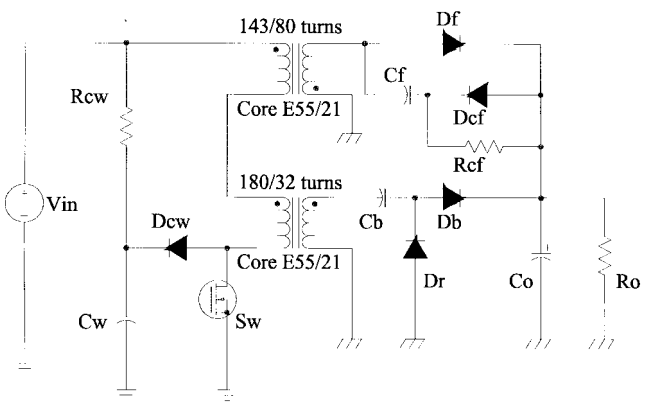

Fig. 10. Power stage diagram of the proposed converter.

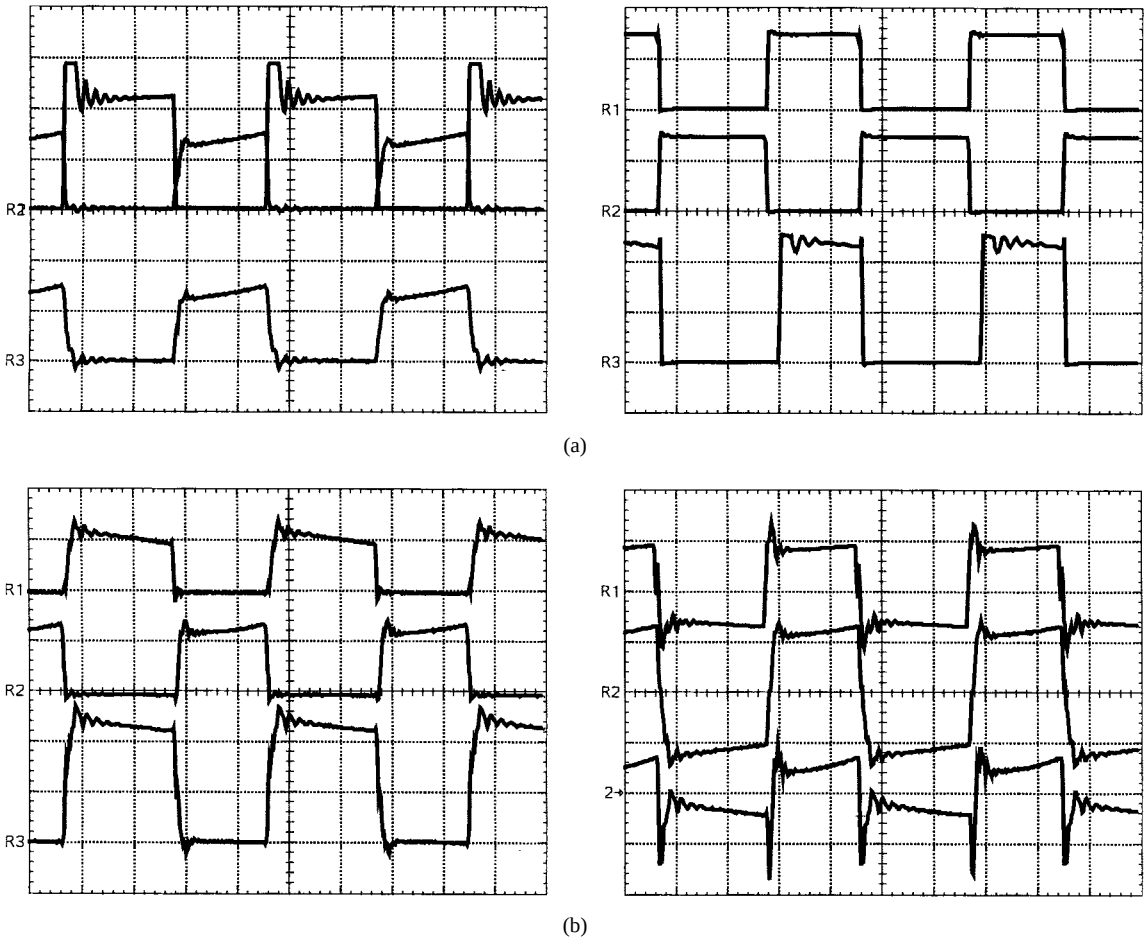

Fig. 11. Experimental waveforms at rated conditions. (a) Upper traces: drain-to-source voltage [250 V/div] and drain current [2 A/div]; lower trace: current through the primary side of the magnetic devices [2 A/div]. (b) Voltage across the rectifier diodes. Upper trace: diode D_r [40 V/div]; middle trace: diode D_b [40 V/div]; lower trace: diode D_f [60 V/div]. (c) Current through the rectifier diodes. Upper trace: diode D_r [5 A/div]; middle trace: diode D_b [5 A/div]; lower trace: diode D_f[2 A/div]. (d) Upper trace: voltage across the secondary side of the transformer [20 V/div]; middle trace: current through capacitor C_b [5 A/div]; lower trace: current ripple through output capacitor [2 A/div]. Time scale: 5 μs/div.

We must take into account the influence of the SRE of C_o on the output-voltage ripple. Thus

$$\text{SRE} \leq \frac{\Delta V_o V_{\text{in}}}{P_o} \frac{D}{n(1-D)-a}$$

$$\text{SRE} \leq \frac{0.01 \times 56 \times 300}{300} \times \frac{0.4}{4.464 \times (1-0.4) - 1.786}$$

$$\text{SRE} \leq 0.251\ \Omega.$$

It has been chosen, for the output capacitor, three units of 330 μF connected in parallel.

VI. Experimental Results

A circuit has been built and measurements were taken from the prototype in order to demonstrate the circuit operation and verify the validity of the analysis.

The power stage diagram of the implemented single-switch flyback-current-fed converter is depicted in Fig. 10. Clamping circuits have been used in order to reduce the effect of the leakage inductance of the magnetic devices on the power switch and on diode D_f. Table II lists the components used in the implementation.

TABLE II
List of Components

Device	Value	Device	Value
R_{ew}	30KΩ/5W	R_{cf}	10KΩ/5W
R_o	10Ω/500W	C_w	1μF
C_f	1μF	C_b	15μF
C_o	3x330μF	D_w	SK4F4/10
D_{cf}	MUR430	D_r	MUR1530
D_b	MUR1530	D_f	MUR1530
S_w	2xBUZ58		

Fig. 11 shows typical converter waveforms in the CCM at rated conditions. The drain-to-source voltage of S_w and its drain current are shown in Fig. 11(a) (upper traces). The current through the primary side of the magnetic devices is shown by the lower trace of Fig. 11(a).

Typical rectifier voltage and current waveforms are depicted in Fig. 11(b) and (c). In both oscillograms, we can see the waveforms that are related to D_r (upper trace), D_b (middle trace), and D_f (lower trace).

Fig. 11(d) shows the voltage across the secondary side of the transformer (upper trace), the current through C_b (middle trace), and the current through the output capacitor. The last mentioned waveform confirms one of the most

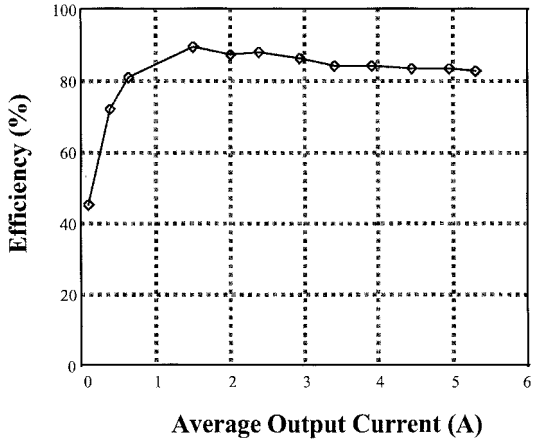

Fig. 12. Efficiency curve for the proposed converter.

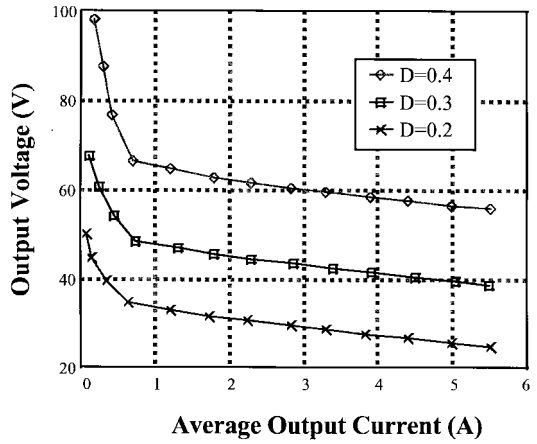

Fig. 13. Experimental output characteristics.

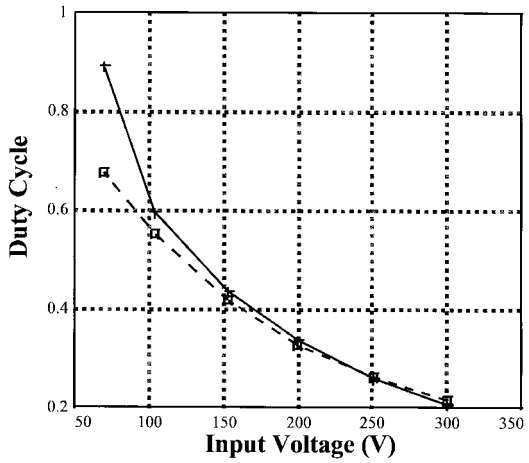

Fig. 14. Theoretical (dashed line) and experimental (solid line) duty cycle for input-voltage variation.

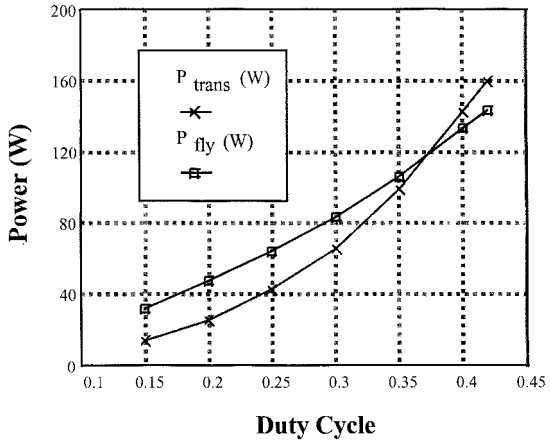

Fig. 15. Power sharing between transformer and flyback inductor.

important advantages of the proposed converter—the low-output capacitor current ripple. This feature is accomplished because in the CCM there always is at least one rectifier diode (D_b or D_f) delivering energy to the output.

In Fig. 12, the efficiency curve as a function of the output current is presented next. The measured efficiency at rated conditions was approximately 82%. It is possible to enhance the efficiency at rated conditions by reducing the leakage inductance of the magnetic devices and improving the characteristics of the semiconductors.

The experimental output characteristics, showing the output voltage as a function of the output current and taking the duty cycle as parameter, are graphically depicted in Fig. 13. The changing in the duty cycle controls the power transferred to the load and regulates the output voltage. The slope presented by the experimental characteristics in the CCM is due to the on resistance of S_w, the voltage drop across the rectifier diodes, and the leakage reactance voltage drop.

Fig. 14 shows a comparison between the predicted (dashed line) and measured (solid line) duty cycle for the input-voltage variation. This curve was obtained to show the ability of the converter to regulate the output voltage in a wide input-voltage range. Particularly, in this case, the input-voltage variation was 5:1. In Fig. 14, the input voltage was changed from 60 up to 300 V, and the operation duty cycle was adjusted to regulate the output voltage to 30 V for constant output power. Note that the theoretical and experimental duty cycle differ from each other for low-input voltage because in this case the input current increases, and, consequently, the losses inside the converter will also increase.

Fig. 15 shows the power sharing between the magnetic devices as a function of the duty cycle. We observe an equalization of the power for a duty cycle around 0.38, close to the value chosen in the design section.

VII. Comparison Between Flyback and Proposed Converter

In this section, we will compare some characteristics between the proposed converter and the flyback one. To simplify the discussion, we will assume that the turns ratio of the magnetic devices of the proposed converter are both equal to n. The analysis will also assume that the input voltage, output voltage, and the power processed by the converters are the same, so the average input current of both converters will be the same. Table III shows the main relationships to be discussed here. In order to refer to the flyback converter, the subscript "f" was used in the expressions.

TABLE III
COMPARISON BETWEEN FLYBACK AND PROPOSED CONVERTER

Item	Flyback Converter	Proposed Converter
DC voltage gain	$\frac{n_f V_o}{V_{in}} = \frac{D_f}{(1-D_f)}$	$\frac{nV_o}{V_{in}} = \frac{D}{(1-D^2)}$
Switch voltage stress	$V_{swf} = \frac{1}{1-D_f} V_{in}$	$V_{sw} = \frac{1}{1-D} V_{in}$
Switch *rms* current	$I_{rmsf} = \frac{I_{in}}{\sqrt{D_f}}$	$I_{rms} = \frac{I_{in}}{\sqrt{D}}$
Output capacitor current ripple	$\Delta I_f = n_f \frac{I_{in}}{D_f}$	$\Delta I = n I_{in}$

To interpret the relationships of Table III, we must take into account two different design strategies: to design the converters for the same dc voltage gain or to design them for the same switch voltage. In the first strategy, for the same dc voltage gain, we can easily see that $D_f < D$. Thus, we will have the same turns ratio for both converters. From Table III, we can conclude that the voltage across the switch of the proposed converter will be larger than the voltage across the switch of the flyback. However, to compensate this disadvantage, the *rms* current through the power switch and the current ripple through the output capacitor of the proposed converter will be lower if compared to the flyback converter, consequently, the power losses in these devices will be reduced in the proposed converter. In the second design strategy, to subject the switches of both converters to the same voltage, it is necessary to have $D_f = D$, then $n_f > n$. In this case, the dc voltage gain of the flyback converter will be larger than the gain of the proposed converter. On the other hand, the voltage and the *rms* current through the power switches of both converters will be the same. The advantage of the proposed converter over the flyback is that the output capacitor current ripple will be lower, reducing the volume of capacitors to filter the output voltage.

In both strategies, the main advantage of the proposed converter is the low current ripple through the output filter capacitor. Therefore, the second strategy is advantageous for the proposed converter because in this strategy both converters are subjected to the same voltage and current stresses.

The overall efficiency of the proposed converter will be lower than the efficiency of the flyback because the proposed converter has two rectifier diodes, one capacitor, and one magnetic device more than the flyback converter. It is easy to show that the current ripple through C_b is lower than the ripple through the output capacitor of the flyback converter, so it is possible to use an electrolytic capacitor to implement C_b.

Finally, another advantage of the proposed converter is the possibility of sharing the output power between the magnetic devices. This characteristic makes the proposed converter to operate at higher power levels than the flyback converter.

VIII. CONCLUSION

This paper introduced an analysis of the properties and operational characteristics presented by a novel single-switch flyback-current-fed dc–dc converter.

The main features of the discussed topology are: single power switch, isolation, single-input inductor, purely capacitive output filter, and operation at constant frequency in a conventional pulse-width-modulation scheme. In spite of using only one power switch, instead of two, the proposed converter preserves the major advantages of the conventional flyback-current-fed push–pull topology.

Operation, theoretical analysis, design example, and experimental evaluation were taken from a prototype rated at 300 W/50 kHz. Along the theoretical analysis was shown that the single-switch converter is appropriated to operate over a wide input-voltage range, which makes it suitable to be used in power factor correction. The main advantage of the proposed converter over the flyback converter is the low current ripple through the output capacitor.

REFERENCES

[1] V. J. Thottuvelil, T. G. Wilson, and H. A. Owen, Jr., "Analysis and design of a push–pull current-fed converter," in *IEEE PESC Rec.*, 1981, pp. 192–203.
[2] R. Redl and N. Sokal, "Push–pull current-fed multiple-output regulated wide-input-range dc/dc power converter with only one inductor and with 0 to 100% switch duty ratio: Operation at duty ratio below 50%," in *IEEE PESC Rec.*, 1981, pp. 204–212.
[3] V. J. Thottuvelil, T. G. Wilson, and H. A. Owen, Jr., "Small-signal modeling of a push–pull current-fed converter," in *IEEE PESC Rec.*, 1982, pp. 224–239.
[4] J. Albrecht, J. Young, and W. A. Peterson, "Boost–buck push–pull converter for very wide input range single stage power conversion," in *IEEE APEC Rec.*, 1995, pp. 303–308.

Peter Mantovanelli Barbosa (M'96) was born in Cianorte, Paraná, Brazil, in 1969. He received the B.S. degree in electrical engineering from Federal University of Uberlândia, Minas Gerais, Brazil, in 1992 and the M.S. degree in electrical engineering from Federal University of Santa Catarina, Florianópolis, Brazil, in 1993.

Since August 1995, he has been working as an Assistant Professor at the Department of Electrical Engineering, Federal University of Paraná, Curitiba, Brazil. His research interests are in the areas of dc–dc converters, power factor correction, electronic ballasts, and UPS systems.

Mr. Barbosa is a Member of SOBRAEP, the Brazilian Power Electronics Society.

Ivo Barbi (M'78–SM'90) was born in Gaspar, Santa Catarina, Brazil, in 1949. He received the B.S. and M.S. degrees in electrical engineering from Federal University of Santa Catarina, Florianópolis, Brazil, in 1973 and 1976, respectively, and the Ph.D. degree from the Institute National Polytechnique de Toulouse, Toulouse, France, in 1979.

He Founded the Brazilian Power Electronics Society and the Power Electronics Institute (INEP) of the Federal University of Santa Catarina. Currently, he is Professor of the Power Electronics Institute. Since January 1992, he has been an Associate Editor in the power converters area for the IEEE TRANSACTIONS ON INDUSTRIAL ELECTRONICS.